Clast rind-paleosol record of the Antarctic early Alpine glaciation

William C. Mahaney [a,b,*], Stéphane Schwartz [c]

[a] Quaternary Surveys, 26 Thornhill Ave., Thornhill, Ontario, Canada
[b] L4J1J4 and Department of Geography, York University, 4700 Keele St., N. York, Ontario, M3J 1P3, Canada
[c] ISTerre, Univ. Grenoble Alpes, Univ. Savoie Mont Blanc, CNRS, IRD, IFSTTAR, 38041, Grenoble, France

ARTICLE INFO

ABSTRACT

The early Alpine glaciation is known from few sources detailing initial growth of ice either during the late Oligocene or early Miocene, localities limited to high summits of East Antarctica. The Ant-831 paleosol, developed in moraine emplaced during the Alpine event, has been studied with respect to its pedogenesis and to rinds recovered from its pebble pavement. This pedostratigraphic section is assigned a late Oligocene/early Miocene age on the basis of its fossil Coleoptera fauna and tundra vegetation, Fe/Al relative-age-dating parameters, and extensive pebble clast weathering. SEM, XRD and XRF analyses of rind specimens from the pebble pavement yield new information on the weathering history of the Beacon sandstone and its link to a juxtaposed paleosol. The paleosol provides a mirror image to weathering zones in pavement clasts, the salt-rich zones interpreted to have formed during the cold-dry paleoclimate of the post-Middle Miocene Climatic Optimum (MMCO ~15 Ma) following a stronger oxidizing paleoclimate of the earlier cold-wet phase of the Alpine glaciation. Essentially this database provides a 30-Myr window into the weathering progression from inception of the Alpine glaciation, through the warmer MMCO dated to ~15 Ma, to the onset of cold-dry conditions that brought on the later development of the Inland Ice Sheet.

1. Introduction

Glaciers are among the most responsive indicators of climatic change and continental ice sheet growth is among the most difficult to document primarily because, with subsequent advance, the deposition record of transition from inception of glacial conditions to production of a fully formed glacier is largely destroyed by erosion. However, in Antarctica (Fig. 1A) the initial start up to glaciation, which began in the high mountains of East Antarctica (Fig. 1B), with the growth of warm-based ice (Marchant et al., 1993; Bo et al., 2009), here termed the early Alpine glaciation, left moraines in place to record subsequent events as warm-based ice transitioned through a cold-dry climate to a fully developed Inland Ice Sheet. Single moraines and moraine stacks in the high mountains stand as silent sentinels recording the long and slow transition from wet-based to dry-based glaciation. Moraines, similar to the Ant-831 section (Fig. 2A and B), emplaced by the Alpine glaciation, consisting of pebbly, sandy-silt sediment, slowly responded to strong wind action leading to production of ventifacted clasts and slow winnowing of fines leaving a pebble pavement of ~3–10 cm thickness. As the pebbly, sandy substrate weathered into a thin tundra-like soil in

transition to a paleosol as climatic cooling progressed, clasts in pebble pavements began collecting environmental information documenting the weathering transition from salt-poor and cold-humid conditions to salt-rich and cold-dry climate. This transition occurred from the late Oligocene-early Miocene through the mid-Miocene Climatic Optimum (MMCO) (Warny et al., 2009) of ~15 Ma (Graham et al., 2002), thereafter entering a cold phase lasting with minor tribulations to the present where climate is responding over the last few decades to the pressures of global warming (Wunderling et al., 2020).

Despite the wide age range for the MCO (Miocene Climatic Optimum) provided by ANDRIL-2 published results, the data reported here fit closely to age ranges reported by Lewis et al. (2008) and Warny et al. (2009) and follow from the one ~15 Ma age reported for the New Mountain embayment sites (Ant-828 and Ant-829). Hence, a designated MMCO is preferred rather than the broad ranged MCO. Continuing the long-argued debate over climatic change in the Antarctic Dry Valleys, Dickinson et al. (2012) showed the weathering system froze between 6 and 9 Ma somewhat younger than estimates presented here and by Lewis et al. (2008).

Pebble clasts in pavement overtopping single paleosols such as Ant-

831 (Fig. 2A), in some instances relatively undisturbed over time with stable clast x-y coordinates (i.e. uniform clast orientation), record slowing weathering processes from early stages with occasional snow-melt, early release of oxides, hydroxides and clay minerals locked in zones inward to the rock core (Mahaney and Schwartz, 2016), to post-MMCO conditions at the New Mountain site (Fig. 1B), with a cold-dry climate producing salt buildup in weathering rinds. The development of weathering zones within pebble clasts to thicknesses of ~25 mm mirrors in some cases, the development of horizons in juxta-posed paleosols, pedons reaching depths of ~50 cm (Mahaney et al., 2001). While this mirror-effect has been noticed in middle latitude alpine sites (Mahaney et al., 2013), its occurrence in the Antarctic (Mahaney, 2019), given the immense difference in time between sites, is astounding. While rinds have proved useful in relative-dating exercises (Nelson, 1954; Sharp, 1969; Birkeland, 1974; Mahaney, 1978), and as archives of cosmic airbursts (Mahaney and Keiser, 2013; Mahaney et al., 2018), exploration of the internal composition and isotopic dating had to wait for the development of new high resolution equipment –SEM/EDS, FIB, STEM etc. –to fully explore (Mahaney et al., 2016) the innards of rinds. Using such high resolution instrumentation on samples

of increasing age, the existence of complex laminae and larger lenses reveal (Mahaney et al., 2012) the molecular enormity of biologic and geologic networks at work in the weathering process. Indeed, with age, rinds in temperate localities tend to carry 'exotic' biologic materials such as lichen rhizines, cellulose and wood in various stages of diagenesis, closely interwoven with a range of lithologies. Whereas we did not observe algae or endolithic lichens in the Ant-831 samples (Fig. 2B), such occurrences in rinds are known in the Transantarctic Mountains and their role in chemical weathering of granite is well established (Guglielmin et al., 2005).

Surficial rinds in contact with the subaerial environment (atmosphere, hydrosphere and biosphere interactions) record all or most imports of matter and energy over time (Mahaney and Keiser, 2013; Dorn et al., 2017; Mahaney et al., 2018) but fail to record losses from the clast surface to surrounding deposits. That additions to the rind front outweigh losses over time is evident, as rinds tend to become thicker with age, with most exhibiting varying numbers of complex weathered zones with distance toward the rock core contact. The rock/atmosphere interface may stay relatively porous and open to the influence of water and heat to maintain the chemical kinetics necessary to allow
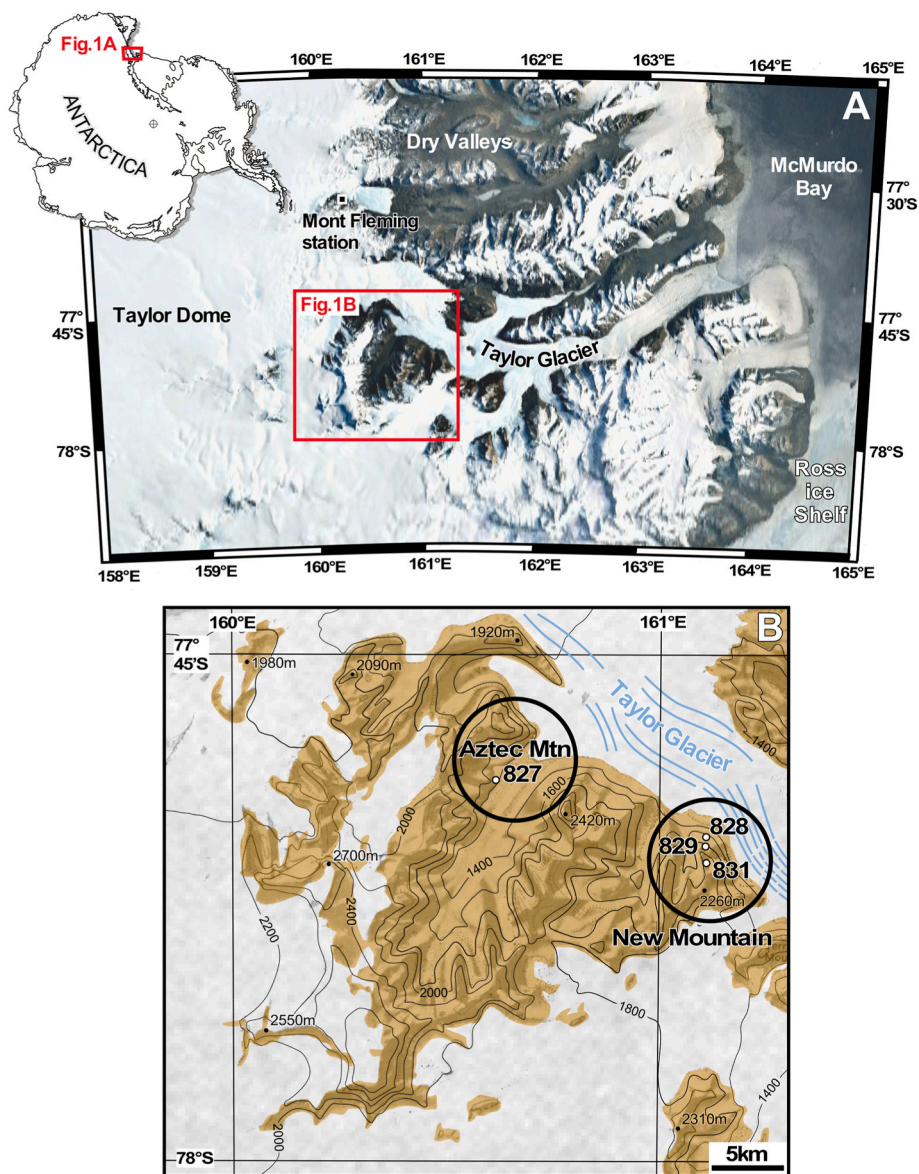

Fig. 1. A, General map of Antarctica showing the Ross Sea and the location of the study area in red. B, Location of the Ant-831 paleosol and other sites (red circle) in the New Mountain and Aztec areas located in upper Taylor Valley.

hydrolysis, oxidation, chelation, hydration and solution processes necessary to release oxihydrites, stray cations etc. leading to the production of clay minerals, salt encrustations, and other alteration products, and even, on occasion, such insoluble compounds as gibbsite. With extreme age the micro-sequence with which some of these weathering products vary, from the rind rim to the clast core, allows paleoenvironmental reconstruction to a fine degree (Mahaney et al., 2012). In the case explored here, the clast weathering reconstruction is inverted to what is in the adjacent paleosol, as indicated by the stack of paleosol horizons with stronger oxides at surface and salt-rich horizons beneath. In virtually all cases studied at New Mountain (Fig. 1B) (Mahaney et al., 2001, 2009), occasional seasonal snowmelt either finds its way into clasts in the pebble pavement or with time through the pebble pavement to the substrate paleosol. This meltwater throughput produces the highest oxidation potential in the surface paleosol horizon or horizons, the least at depth in lower horizons where salt concentration increases.

The question of the rate of weathering and production of alteration products between a pebble clast in the pavement and paleosol sediment in the adjoining substrate, all constrained by an estimated ~30 Myr of time with near continual decline from cold-humid to cold-dry paleoclimate, is the subject of this research. Considering other estimates of the growth of Alpine ice in East Antarctica beginning in the late Oligocene, all based on retrieved cores (Sirius) (Passchier (2004), moraine analysis (Marchant et al., 1993), it is a seminal option and opportune time to add weathering rinds plus paleosols to the database. The preservation of Ant-831 over 30 Ma of time is what gives this location its unique character.

2. Regional geology

Across the broader area of East Antarctica and the Transantarctic Mountains, the Taylor Glacier–New Mountain area (Fig. 1B), is underlain with basement rock comprising granite and gneiss, which in turn are overlain with a complex of sedimentary strata including the Beacon Supergroup as described by Stewart (1934) and Shaw (1962). These lithologies include arkosic sandstones intruded in places by doleritic dikes and sills comprising the Ferrar dolerite. Glacial deposits at New Mountain comprise a range of sandstone, dolerite, granite, and gneiss in various proportions. Roundness/angularity measurements were not carried out at the field sites since the mix of sediment includes the Beacon Supergroup with a prevalence of subround to round clasts which would skew any attempt to distinguish Alpine from Inland ice sources, i. e. warm to cold based ice. Field sites include topographic settings alternating from steep ridges and slopes to benches, all of which comprise a landscape similar to South Africa where these surfaces formed originally under an arid climate (Campbell and Claridge, 1987; Mahaney et al., 2001).

The area around the McMurdo Ice Shelf (Fig. 1B) features volcanic terrain dating from 10 to 15 Ma based on work by Armstrong (1978), with the landscape only partly modified by glacial and mass-wasting processes. Mount Terror, one of the major landmarks in the Ross Island area, and other nearby mountain massifs, have suffered only minor modification by glaciation and mass wasting processes. As indicated later, the pebble pavement in the Ant-831 section yields clasts with a salt complex on surface, oxide/hydroxide release beneath, which suggests marginal clast disturbance because the salt has a marine origin and would be expected to form on clast surfaces. A wide area of the Transantarctic Mountains, floored with granitic basement, is sculpted with former erosion surfaces covered with younger formations collectively named the Beacon sandstone based on outcrops near the Taylor Glacier (Fig. 1B), after work done by Ferrar (1907). The original sandstone assignment was later integrated to comprise a wide range of clastic rock from conglomerate to siltstone, all of which transition upward into massive beds of quartz-rich sandstone spanning the Devonian to Jurassic. Several workers, including Campbell and Claridge (1987), Barrett (1981), and Bradshaw (2013), consider these sediments to be sourced from basement rocks of East Antarctica. The sandstone clast analyzed in this case (Fig. 3A) was likely sourced from the Hatherton sandstone, a member of the Taylor group, but without trace fossils intact it is impossible to know for certain. The Hatherton sandstone comprises subaerial features, which include desiccation cracks, raindrop impressions, as well as planar to cross-bedded features owing to a fluvial origin.
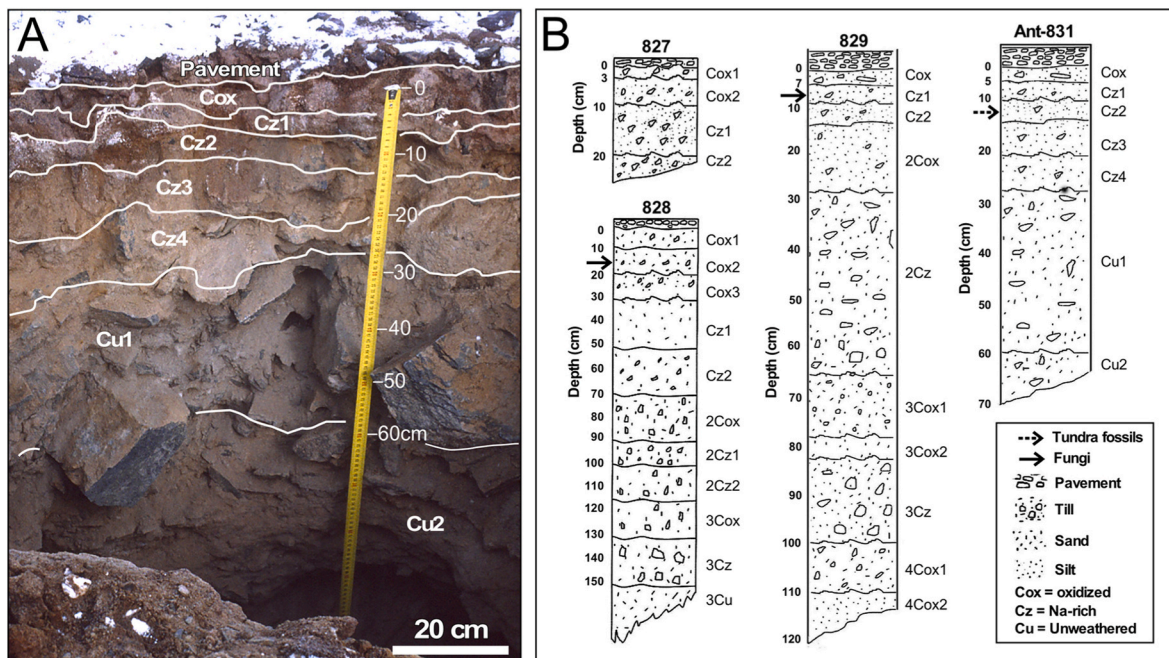

Fig. 2. A, Ant-831 profile with horizons annotated with boundaries more convoluted than shown in B. Reddish grains at depth in Cz4 are spills from above. The presence of boulders marks this section apart from others with tills from continental glaciation; B, The dashed arrow for Ant-831 indicates Coleoptera fossils, part of the tundra landscape that existed during the Early Miocene. The full arrows for Ant-828 and 829 indicate the presence of copious colonies of extant fungi in the mid-upper paleosols. (For interpretation of the references to colour in this figure legend, the reader is referred to the web version of this article.)
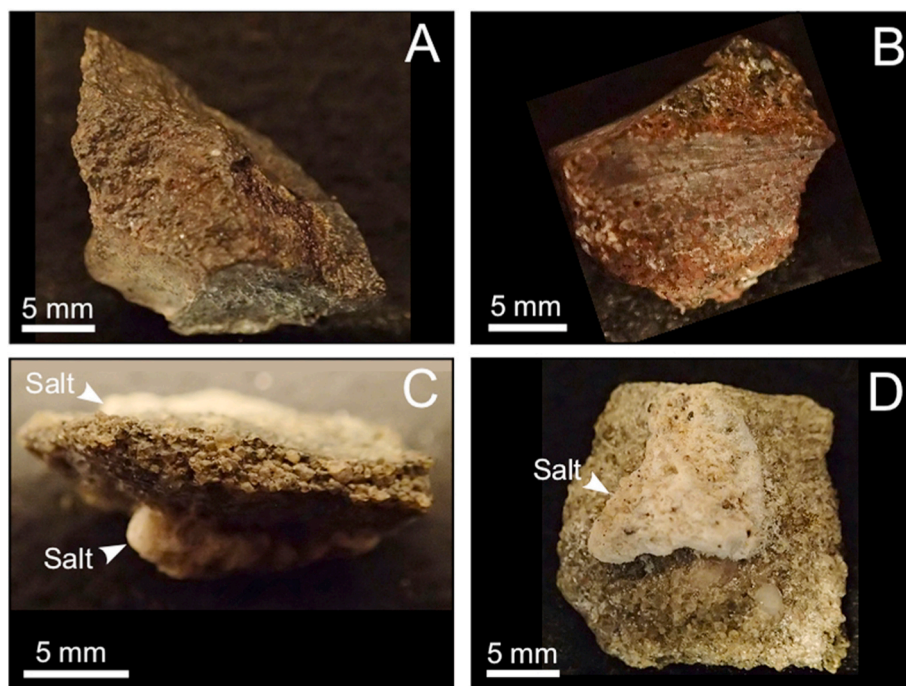
Fig. 3. A, Approximate ~20 mm wide clast with massive rind covering small area of core rock, with Fe–Mn rind of ~4 mm thickness, well ventifacted; B, Rind covering clast with small area of core rock showing mid-photograph. The rind is inverted with top intersecting the paleosol body; C, Salt cover top and bottom showing ~6 mm thick sandstone clast; D, Salt plate covering ~12 mm thick sandstone clast.

According to most workers (Marchant et al., 1993; Lewis et al., 2007; Bo et al., 2009; Denton et al., 2010; Anderson et al., 2011; Passchier, 2011; Mahaney et al., 2014; Mahaney, 2015), the initiation of glaciation in East Antarctica is thought to date from the late Oligocene to early Miocene, and perhaps earlier from the Eocene (Wilson, 1973). Despite the uncertain time of glacial initiation, the onset of warm-based ice began in the highland areas (Campbell and Claridge, 1987), which in turn was followed by the slow growth of cold-based ice at some point during the Miocene (Warny et al., 2009). Following the MMCO and for most of the Late Neogene, climate may have become colder than today but the effect on continental vs alpine ice remains an open question. Recent evidence (Dickenson et al., 2012), of 'the onset of 'frozen hyper-arid conditions' at high elevation (1840 m) on Table Mountain, where water froze between 6 and 9 Ma, implies that warm-based ice may have occupied discrete intervals in the Pliocene and late Miocene. Compared to the older Ant-831 paleosol, the younger moraine surfaces at Aztec Mountain, and in the New Mountain embayments (Fig. 1B), may owe their origin to an influx of cold-based ice during the MMCO or at some time thereafter, as described by Mahaney et al. (2001).

Mass balance changes of the Inland Ice are thought to have produced an influx of ice from outlet glaciers invading elevated benches at New Mountain (Fig. 1B), and nearby localities near Aztec Mountain (Mahaney et al., 2001). Such outlet glacial oscillations were cold-based, their velocity produced by plastic deformation without basal sliding, which likely protected underlying surficial deposits (Owen et al., 2009). If underlying deposits remained frozen, such surficial deposits were afforded protection from erosion, thus movement of ice left moraines and buried paleosols at New Mountain well preserved, all of which supports the cold-based ice incursion hypothesis. Periodic incursions of ice from the Taylor Glacier (Fig. 1A), caused by mass-budget changes, with ice overtopping valleys and flowing into embayments, is evident with moraine deposits exhibiting stratigraphic successions which record multiple deposition/weathering events occurring sometime in the middle Miocene (Mahaney et al., 2001). However, oscillating ice incursion events at the New Mountain embayments, as illustrated by the pedostratigraphy in Fig. 2B, are characteristically different from the Ant-831

site which is part of a moraine complex at higher elevation that produced a single end moraine followed by a long period of weathering that stretched through the early Miocene, the MMCO of ~15 Ma, and on into the Neogene.

3. Materials and methods

3.1. Field sedimentary analysis

Situated above the embayment sites at New Mountain, the Ant-831 section is located in an end moraine (Fig. 1B) (coordinates - 77° 51′ S; 161° 09′ E). Unlike the multi-stacked paleosols at other sites (Mahaney et al., 2001; this paper Fig. 2B), near New Mountain–-Ant-828, Ant-829 (Fig. 1B)— which date to the MMCO, the older moraine deposit at Ant-831 (Fig. 2A) contains a single-stack paleosol with an overlying pebble pavement deposited at some time during the initial Alpine glaciation. The samples under investigation include parent material (Cu), overlain with salt-rich horizons (Cz) and a Fe-spiked zone (Cox), the profile overtoped by a 3-10 cm-thick pebble pavement, a succession similar to the other sections lower down and at Aztec Mountain (Mahaney et al., 2001; Mahaney and Schwartz, 2016). The site, hand dug in dry frozen sediment to just above an ice table, was sampled to expose all horizons, including the pebble pavement to depth where all undifferentiated, unweathered parent material could be collected. The samples were airlifted to Toronto for lab study as indicated below. All paleosol horizon designations reported here (Fig. 2A and B) are genetic and follow normal horizon nomenclature previously reported by Mahaney et al. (2001 and 2009), as adapted from NSSC (1995). The usual downward succession of horizons (weathered beds) follows from Fe-rich sediment transitioning to salt-rich sediment, that is, Cox to Cz horizons, which follows the US soil classification system (NSSC, 1995; Birkeland, 1999; Soil Survey Staff, 1999). When oxidation effects are stronger than 10YR 5/4 (color based on Oyama and Takehara, 1970), an 'ox' designation (Birkeland, 1999) is used; hence, Cox becomes the usual surface horizon or part of a subset of horizons. To decipher color variations according to the Munsell System, see Millar et al. (1966), who specify standard observation and recording techniques. The "u" designation for unweathered C horizons follows from horizon nomenclature

introduced by Hodgson (1976).

3.2. Laboratory analytical analysis

Once in the laboratory, paleosol samples were air-dried and sieved to separate pebble grade size material from the 2-mm fraction, the latter comprising bulk sediment samples used for analysis. To determine water content, the bulk sample was subsampled using 10 g of material weight, heated to 110 °C. The air-dry weight/oven-dry weight ratio was used to determine the moisture factor x 50 g to determine the air-dry equivalent of a 50 g oven-dry sample, to comply with ASTM procedures. In lieu of oven-dried weight often used for particle size analysis, this air-dry equivalent weight was used in the particle size analysis of each sample. Samples were lightly sonicated to clean sands, but with low to nil organic content, 30% H_2O_2 was not applied to remove organic matter. Also, with low clay content, Na-pyrophosphate was not considered necessary for deflocculation. Following these initial steps, samples were wet-sieved to separate sand from silt-plus-clay; the sands dried at 110 °C and sieved to weigh out the five sand fractions. The oven-dried sands were separated into coarse (2000–250 µm) and fine (250–63 µm) fractions and retained for microscopic analysis. Using a fine needle, sands (in Figs. 7–10) were handpicked and placed on stubs either with colloidal glue or using sticky tape, and later analyzed without coating on

a Hitachi scanning electron microscope (SEM), model S-4500. Samples in Fig. 6A–D were analyzed on a TESCAN VEGA-3 SEM operated at 16 kV and equipped with a RAYSPEC EDS detector (SSD 30 mm²). Rare earth elements and total and extractable Fe and Al were analyzed using the bulk <2 mm fraction at the former SLOWPOKE nuclear reactor at the University of Toronto using appropriate standards as outlined by Hancock (1984) and Harrison and Hancock (2005). Iron and Al extractions were analyzed by atomic absorption spectrophotometry using a Perkin Elmer 373 AAS following procedures outlined by Mahaney (1990).

Chemical mapping of the rind sample (Fig. 4B) was realized using a Micro-X-ray fluorescence EDAX Eagle III spectrometer at ISTerre (Grenoble, France). The Rh anode, operated at 400 µA, used an acceleration voltage of 20 kV, which produced a fluorescence spectra measured with an energy-dispersive X-ray detector at a resolution of 140 eV. Chemical maps were realized with a matrix of 256 × 200 pixels with a 40 µm step-interval in x,y directions, and a dwell time of 1 s per pixel. The color scale for each map corresponds to the intensity of the Kα-lines of the different elements (Si, Al, S, Fe).

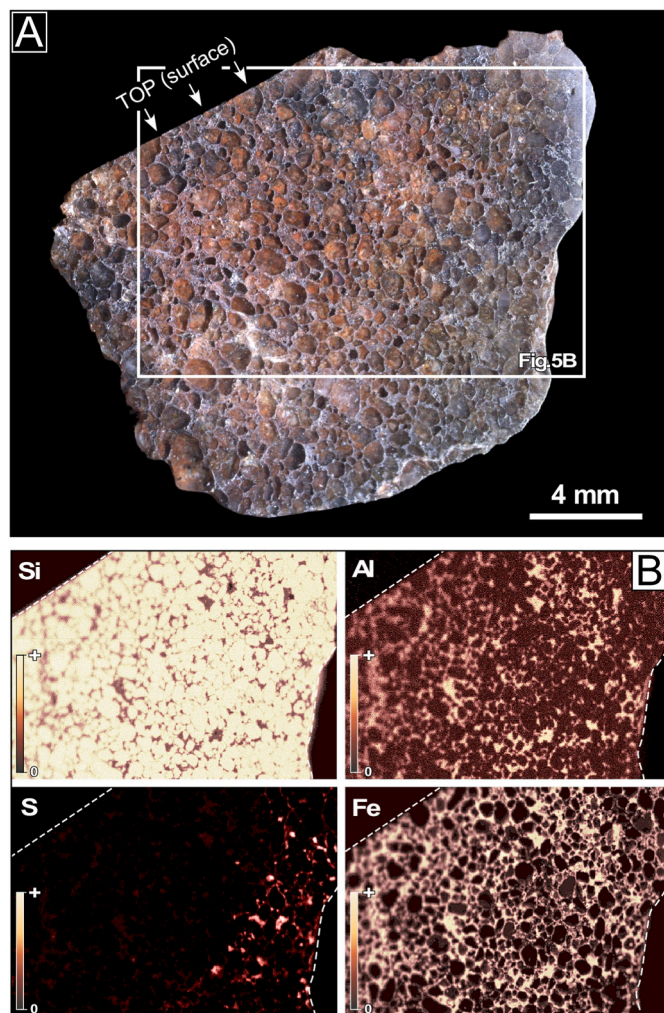Rind samples were further ground and wet sieved to separate sands

Fig. 4. A, Enlarged sandstone clast image of the polished specimen; B, Mapped elemental distributions by XRF analysis show widespread concentrations of Si–Al–S and Fe. The Si content corresponds to the grain quartz whereas the Al and Fe content correspond to the clay matrix. Sulphur limited to the right margin in a rind segment may relate to gypsum.
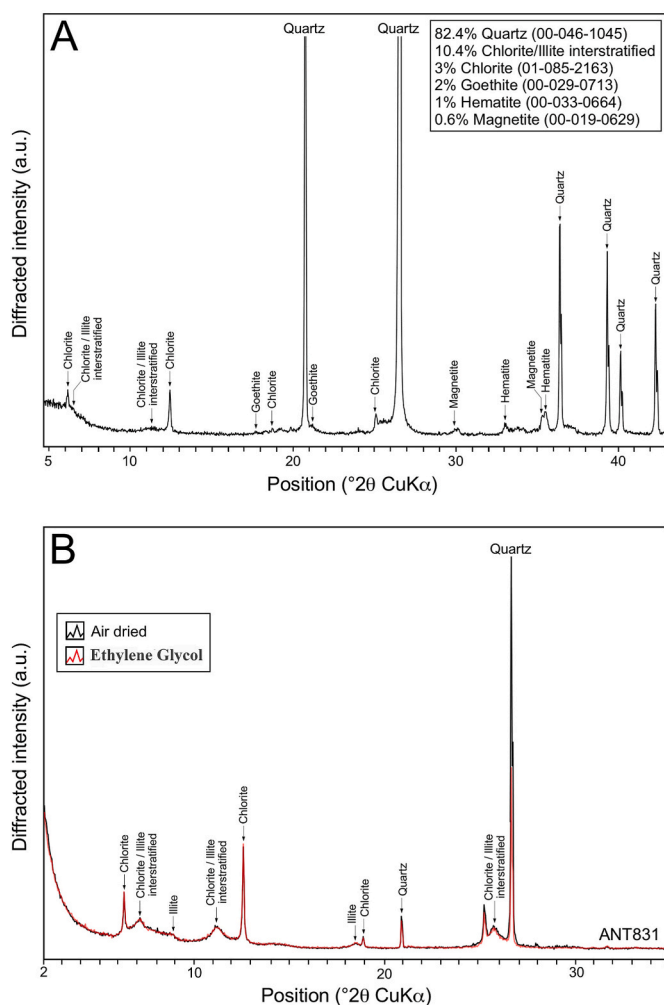

Fig. 5. A, XRD diffractograms of the bulk (<2 mm) fraction of the Ant-831 sample and the XRD standard phase numbers from International Centre for Diffraction Data base (ICDD) are indicated. The estimated quantification of the phases are indicated and carried out by modeling X-ray diffractograms (Rietveld refinement method). B, XRD diffractograms of the clay (<2 µm) fraction of the sample Ant-831. Pattern recorded under air-dried conditions is shown as solid black lines, whereas those recorded after ethylene-glycol salvation is shown as solid red line. (For interpretation of the references to color in this figure legend, the reader is referred to the Web version of this article.)
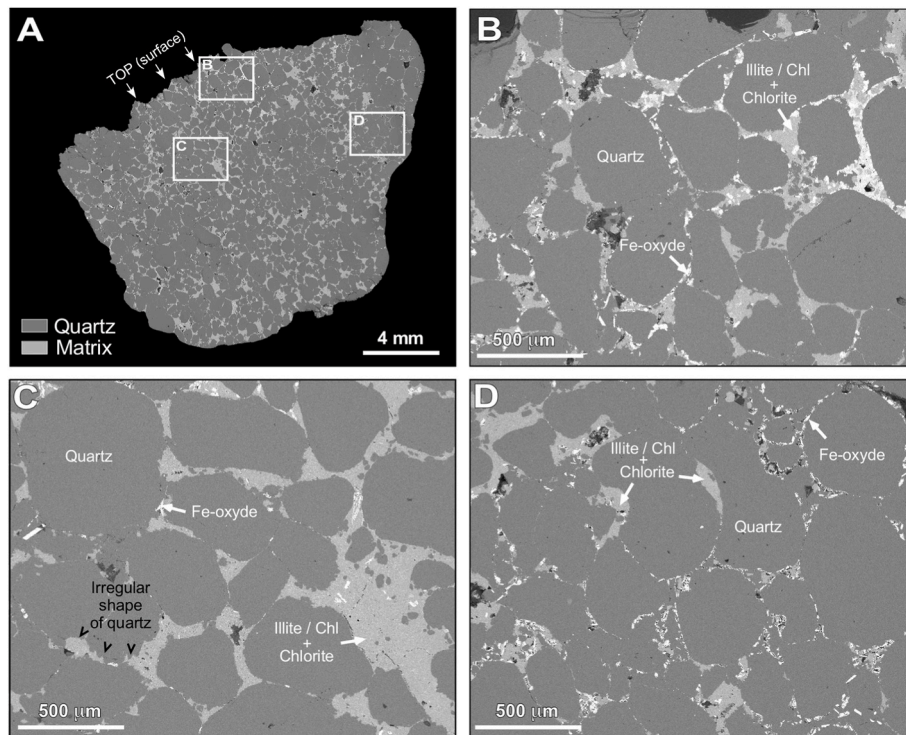
Fig. 6. SEM images of the Ant-831 clast. A, Image of the entire sample surface showing quartz grains embedded within a clay mineral matrix. The location of the images B, C and D are indicated. The shapes of the quartz grains are irregular (B, C) indicating dissolution processes. The matrix is composed of chlorite and illite/chlorite interstratified with locally the development of Fe-oxide within the boundary of the quartz (D).

from clay and silt. The fraction <2 mm was ground using a McCrone micronizing mill, and prepared as a randomly oriented mount. The clay mineralogy was determined on the <2 μm fraction extracted by centrifugation and prepared by drying the resulting suspension onto glass slides. The slides were exposed to Ethylene-glycol (EG) vapor at 70 °C for a minimum of 12 h. The XRD spectra were obtained by using a Bruker D8 diffractometer equipped with a SolXE Si(Li) solid state detector using CuKα 1 + 2 radiation. Intensities were recorded at 0.026° 2-theta step intervals from 5 to 90° for the bulk and from 2 to 50° for the clay (<2 μm) fraction. For the bulk fraction, the quantification of the different mineralogical phases was obtained by modeling X-ray diffractograms (Rietveld refinement method).

4. Results and discussion

4.1. Ant-831 pedostratigraphy

Similar to other paleosols at New Mountain embayments and at Aztec Mountain (Fig. 1A and B), the paleosol at Ant-831 weathered to its present state by concentrating salt in Cz horizons, overlain with horizons concentrating higher amounts of Fe. What differs at Ant-831 is the pebble pavement with weathered clasts carrying rinds with robust colors in the 2.5YR and 5YR ranges indicating thick reddish-brown coatings, contrasted with lower grade (lighter) color in the paleosol, as explained later in the manuscript. Whereas the weathering of a bed within a multistory paleosol (Fig. 2B, sites 828–829), such as in the lower embayments, represents a short time interval to be finally buried by renewed glacial deposition, the buried paleosols lack pebble pavements, with only the youngest glacial incursion depositing a pebble bed. Thus, with full pedostratigraphic successions such as exist at sites Ant-828 and 829 (Mahaney et al., 2001), the absence of pavement separating each buried paleosol lessens time of weathering between each buried unit. As clast weathering in pebble pavements progressed in tandem with weathering in juxtaposed deposits forming into paleosols, the same

scenario unfolded with sections lacking buried units such as at Aztec Mountain and the higher elevations at New Mountain. The paleosol produced at Ant-831, and in the surface of other multistory pedostratigraphic sections belong to the cold-desert class of Antarctic soils identified by Campbell and Claridge (1987) and others (Bockheim, 2007, 2013; Mahaney et al., 2009). Similarly, the paleosol moisture regime in Ant-831, and in other profiles at Aztec Mountain and in the New Mountain embayment, are considered xerous to subxerous, that is, measurably drier than in the pedons of coastal Antarctica, sites with higher temperature and precipitation (Campbell and Claridge, 1987). Melting of summer snowfall tends to wet pebble pavements as well as the upper horizons of adjacent paleosols producing saline water that is known to exist as intergranular films (Ugolini and Anderson, 1973; Cuffey et al., 2000; Wynn-Williams and Edwards, 2000), thus facilitating weathering to operate at temperatures well below 0 °C. Ugolini and Anderson (1973) proved that even with intense freezing, ionic transfer of salts in solution may occur through coatings on sand/silt grains.

This late Oligocene/early Miocene-age paleosol (Ant-831) lies embedded in a moraine outcrop of the Alpine glaciation near New Mountain, Antarctica, as a long-lived record of initial weathering during the start-up of cold-humid climate that lasted for some ten to fifteen million years. This early warm-based glaciation transitioned at some point into the cold-dry climate that began with the growth of the Inland ice, starting at or around the MMCO based on dated beds in the New Mountain embayment. Without sufficient organic material and lacking sufficient clay, these paleosols are not easily classified using the soil taxonomy (NSSC, 1995) and as a result are best described using normal horizon nomenclature and resorting to distinguishing weathering entities comprising: pebble pavement overlying C/Cox/Cz/Cu horizons; with rare Bw horizons appearing closer to the coast where movement of soluble materials and relative grades of Fe oxides and hydroxides can be shown to form a couplet of Bw/Cox horizons. With limited sufficient organic carbon sourced from relict tundra, paleosols in the Transantarctic Mountains lack A or Ah horizons. While these profiles predate
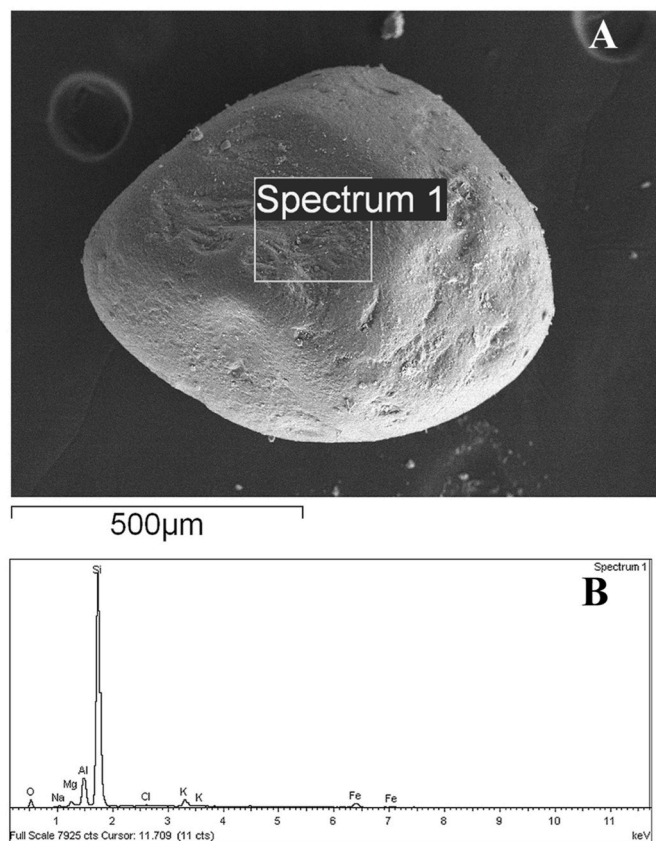
Fig. 7. A, Round coarse quartz grain from the Cz2 horizon in the Ant-831 paleosol. Approximately ~40% of grains in the entire paleosol carry a round classification, most with craters of unknown origin, striae, some chattermark-like microfeatures and occasional v-shaped percussion scars, the latter indicative of water transport. The close association of percussion cracks and striae suggest glaciation with significant meltwater; B, EDS targets include minor Fe coat, Al, Mg and K, with the Al and K indicating an orthoclase composition for minor adhering particles. Grain image and chemistry from Mahaney (2019).

the MMCO, dating such weathered sediment relies on relative-age-dating methods including: elevated Fe and Al extracts as weathering products (Mahaney, 2015), presence of fossil tundra vegetation, Coleoptera typed to cold-warm temperate climate, and presence of deeply entrenched weathering rinds in pebble pavement (Mahaney and Schwartz, 2016).

Rinds collected from this pebble pavement of Alpine-age and sediment at site Ant-831 reveal weathered zones that widely mimic paleosol horizons in adjoining deposits. As shown in Fig. 2B, sediment weathering at Ant-831, as at other sites of similar or younger age, presumably proceeded slowly, producing at least during its early weathering history, a succession of pseudo-Cox to Cz horizons, with horizon differentiation assigned on the basis of Fe development (Cox) versus salt-encrusted (Cz) horizons, separated at the surface with development of a pebble pavement. One rind thickness measured in the Ant-831 section measures ~11 mm over ~30 Ma (Fig. 3A). Because rind weathering zones defy age determination, it is only possible to support a hypothesis that clast weathering began during a time of warmer/moist climate (i.e. the Alpine event), followed across the clast/salt contact by a colder-dry climate. Such a hypothesis is supported by mineral weathering and chemical changes based on findings previously reported by Mahaney and Schwartz (2016) and reconfirmed here with new data that highlight the incorporation of fine clastic components near the lower part of the surface salt encrustation/rock core contact. These incorporated particles, presumably distributed as airfall particles, were eventually taken up by various Na salts, presumably of marine origin (Claridge, 1977;
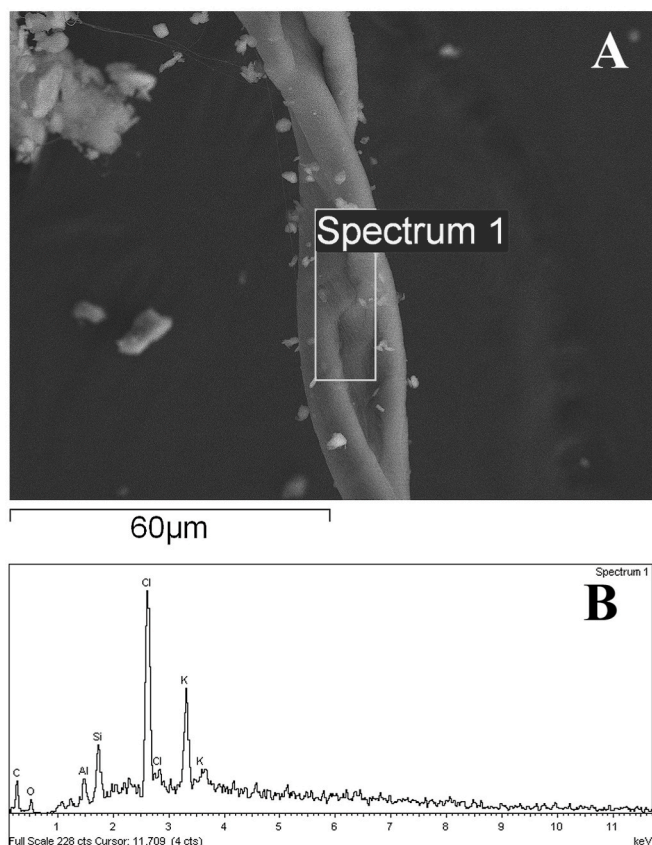

Fig. 8. A, Intertwined fossil root particles presumably from a vascular tundra plant; B, EDS targets sylvite as the main mineral in the fossil with Si:Al at 2:1 with K suggesting accessory orthoclase adhering particles. The C is real and likely some has been lost into the carbon cycle (Duplicate image and chemistry from Mahaney, 2015).

Claridge and Campbell, 1968). Horizons within the paleosol body lie inverted relative to the rind, with salt-rich horizons at base, oxihydrite lightly laden horizons at top, the exact inverse of what is usually found in the pebble pavement and representative of water movement from occasional snowmelt.

4.2. Ant-831 mineralogy

Sands in the Ant-831 paleosol (Fig. 2A and B) are dominantly sub-round with quartz signatures identified by EDS with traces of Al, Fe, S, Ca, Mg and K. Subround grains could result from water or ice abrasion during the cold-humid phase of Antarctic glaciation or inherited from the Beacon sandstone, the dominant lithology in the area of New Mountain (Mahaney et al., 2009). Trace chemical elements are probably weathering products derived from gypsum break-up or from weathering of plagioclase or dolerite minerals. Sands with thin coatings in the paleosol, not energized by EDS, may be clay coatings of unknown composition. The Cz2 horizon in the Ant-831 paleosol also features organo-mineral mats similar to the example in Mahaney (2019) which is a combined weathered mass of aluminosilicates and organics of unknown origin, presumably with bulk carbon lost in the carbon cycle.

Particle size analysis of the Ant-831 paleosol (Fig. 2A–B) reveals sand-silt-clay material placing all horizons within a sand or silty-sand texture (Link, 1966). Sediment color based on Oyama and Takehara (1970) places the surface Cox horizon as dull yellowish brown (10YR 5/4), reflecting the higher content of dolerite. Lower down in mid-section the Cz1 and Cz2 horizons, with mineralogy dominated by granite, sediment color is lighter, reduced by two values and a chroma becoming grayish-yellow brown (10YR 6/2) and dull yellow-orange
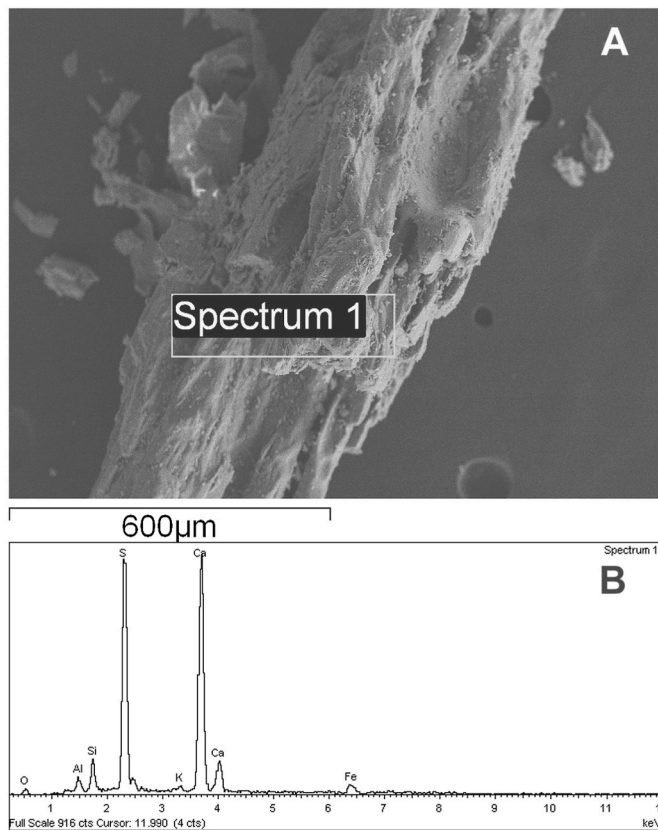
Fig. 9. A, Fossil wood, pith of an unknown plant remarkably well preserved; B, EDS shows plentiful gypsum, minor orthoclase and trace of Fe coating.

Fig. 10. A, Interwoven rootlets in an organic mat with the original carbon lost to the carbon cycle; B, EDS shows some C is real. Si:Al is likely linked to either Ca or K; hence, one or more plagioclase minerals. Cl is probably partly a mix of Na–S salts and Fe is part of the coating. (Duplicate image and chemistry from Mahaney, 2015).

(10YR 6/4), respectively. Lower still in the section, color varies from light gray (10YR 7/1) to dull yellow-orange (10YR 7/3), followed by a transition to light gray (2.5Y 7/1) at depth. As discussed previously by Mahaney et al. (2001), the Cz2 horizon revealed a clay mineral content with significantly higher amounts of smectite compared with other horizons analyzed at New Mountain (Mahaney et al., 2014). Changes of hue from yellow red (10YR) within the paleosol to yellow (2.5Y) in the parent material follows the usual contrast in soils/paleosols where weathered horizons (i.e. the paleosol) differ from unweathered, undifferentiated sediment in the parent material. However, as illustrated here, the weak grayish yellow-brown and dull yellow-orange colors of the paleosol when contrasted with the light gray colors of the parent material underline the inordinately slow conversion of primary minerals to oxides/hydroxides and clay minerals over at least ~30 Myr since weathering began. The strongest colors are likely the product of weathering during the cold/humid pre-MMCO time. Stronger hues in the pebble pavement relative to the paleosol may reflect snowfall/melt pathways from the pavement surface downward.

4.3. Relative age and paleoenvironmental determinations

Well documented paleosols belonging to the early cold-wet phase (Alpine event) of Antarctic glaciation are rare, the only two existing sites coming from research at New Mountain and Mt. Fleming soil climate station (Fig. 1A; Mahaney et al., 2014; Seybold et al., 2009). The New Mountain Ant-831 site contains semi-gelic sediment within the top ~100 cm thickness of the deposit surface, the permafrost (ice table) depth within 200-cm of the surface. The Ant-831 paleosol classifies within the Gelisol order (Natural Resources Conservation Service; http://soils.usda.gov/). Comprising dry frozen sand and with horizons composed of primary and secondary gelic sediment (variable smectite), very low carbon, and no evidence of cryoturbation, the Ant-831 profile
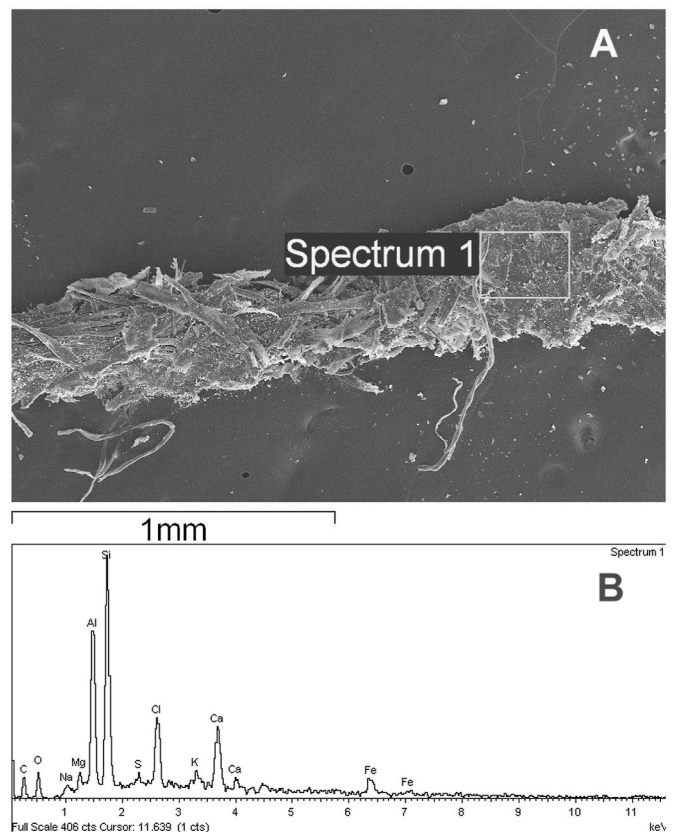
classifies to the Orthel suborder of Anhyorthel, that is, a profile with gravel (pebble bed) over an oxide rich C(ox) horizon coupled with underlying salt-rich horizons (Cz), overlying permafrost. While the properties of the Ant-831 profile bear close similarity to the paleosol at the Mt. Fleming Climate Station adjacent to the Inland Ice Sheet, the geomorphology between the two sites differs because the Mt. Fleming site (Seybold et al., 2009), at 1698 m (77° 32′ S; 160° 17' E), is ~150 m lower than the Ant-831 site, and its profile is within a polygon consisting of coarser sediment compared with the Ant-831 site. However, with a similar depth but slightly stronger 10YR 5/4 colors, the Mt. Fleming paleosol is probably akin in age to the Ant-831 profile or possibly older.

Owing to a lack of recovered tephra, absolute ages for the Ant-831 paleosol are unavailable but if the correlation with Mt. Fleming (Fig. 1A) is correct, the New Mountain paleosol could fall within the range of Sirius deposits that are considered to have age ranges coeval with the early Alpine phase of Antarctic glaciation (Passchier, 2004). Relative age control for the Ant-831 paleosol based on Fe extracts of horizons in the 831 profile—principally Na-dithionite (Fe_d) and acid ammonium oxalate (Fe_o) taken from Mahaney et al. (2009)—have been used to determine relative ages of individual horizons. With known lithologic discontinuities between the surface pebble/Cox beds and subsurface Cz/Cu horizons, age differences may exist between the two subgroups. Moreover, it may also prove possible that sediment at the Ant-831 site was deposited by more than one glaciation with two very different source areas operating over a long but variable length of time. Because the available data are site limited and no exact age is available for the pebble pavement the results are tentative.

Because Fe extraction estimates (Table 1) are the first made, and further, because they are of inestimable value in establishing sediment age

determination (Mahaney, 2015), they underscore the slow rate of conversion of Fe^{+2} to Fe^{+3}. The conversion of primary Fe to secondary forms of Fe is a chief requirement for bacteria and insect respiration (see Fig. 2B for microbe identification, and it is also one of the main electron acceptors for bacteria growth (Hart et al., 2011). Additionally, the use of Fe/Al extracts, proposed by Mahaney (2015) and Mahaney et al. (2009), were made to determine the various weathering products. Acid ammonium oxalate Fe (Fe_o), formerly thought to approximate amorphous Fe (Lutwick and Dormaar, 1973), is now considered (Parfitt and Childs, 1988) to provide an approximation of percent ferrihydrite ($Fe_{10}O_{13}\cdot 9H_2O$). The Fe_o raw data (Mahaney et al., 2009) mark the highest concentrations in the Cox to Cz1 horizons, followed by smaller amounts in horizons lower down-section. Aside from higher concentrations in the profile itself, measurable concentrations in the Cu horizon indicate previous minor weathering (preweathering) of Fe minerals prior to the growth of mountain glaciation, followed by glacial/aeolian transference. The data also indicate that ferrihydrite Fe_o concentrations exceed secondary ferrihydrite, hematite, and goethite (Fe_d) combined, making up over 50% of the three secondary compounds. Ferrihydrite dominates (62%) of the secondary Fe minerals, whereby its adsorbed water might possibly have been utilized by formerly present insects/microbes. The higher values of Fe_o and Fe_d in the Cox horizon are partly a reflection of the lithology with higher dolerite in the surface, the combined Fe_d comprising ~20% of the total Fe (Fe_t). Because higher Fe_o over Fe_d in the Cz1 horizon is troublesome, it possibly results from an incomplete extraction of one or the other secondary form.

The Na-dithionite Fe extract (Fe_d), as pioneered by Mehra and Jackson (1960), approximates the major forms of secondary Fe, principally the combination of ferrihydrite + goethite + hematite. The ratio of Fe_d/Fe_t among the horizons (Table 1) provides an estimate of the conversion of primary Fe (Fe_t) to secondary forms of Fe which nearly doubles from the Cox to Cz2 horizon, this lower horizon is where fossil tundra flora and fauna resided (see section 4.7). This difference between horizons in the paleosol follows from Fe mineral content determined by sand counts made with the light microscope and SEM. Despite the differences in the concentration of primary Fe (Fe_t) between the Cox and the Cz2 horizon, it appears that the Ant-831-Cox vs. Cz horizon group received about the same release of secondary Fe over the ~30 Ma weathering time. Moreover, the Fe concentrations in the Cz2 horizon show that 62% of the Fe_t has been weathered to secondary Fe_d. Despite the total Fe (Fe_t) difference between both horizons – Cox to Cz2 – there may well be little difference in age between both horizons.

The correlation of organic carbon with Al_p (Table 1) (Mahaney, 2015), a relationship suggested by Parfitt and Childs (1988), shows very minor concentrations of Al_p throughout the profile, but with nil organic carbon measured (by LOI) in only two horizons (Cz2 and Cz4). Clearly, since Al_p approximates organically-complexed compounds, it may be that Al armors organic constituents in a fashion similar to Fe and complexated organic materials (Eglinton, 2012), or that the organic carbon concentrations are so minimal that Al_p does not complete a full extraction.

4.4. Pre-weathering and pre-Alpine grain transport

Thin Al coatings on grains in Ant-831 may relate to a grain's pre-weathered history, that is, its previous presence in an aggressive

Table 1
Distribution of Fe – Al in the Ant-831 sample.

Soil horizon	Soil depth (cm)	Fe_o (%)	Fe_d (%)	Fe_t (%)	Al_p (%)	Fe_d/Fe_t
Cox	0–5	0.31	0.48	0.77	0.04	0.17
Cz1	5–9	0.17	0.14	0.51	0.02	0.27
Cz2	9–14	0.10	0.16	0.50	0.02	0.32
Cz3	14–21	0.10	0.18	0.46	0.01	0.39
Cz4	21–27	0.10	0.17	0.55	0.04	0.31
Cu1	27–60	0.06	0.04	0.33	0.01	0.12

leaching environment (pre-MMCO, or pre-Alpine); hence, the presence of Al coatings may relate to gibbsite as weathered by leaching of Si from clay minerals as described by Mahaney (1990). The SEM imagery described by Mahaney (2015) illustrates the variety of subround to subangular grains observed in the Ant-831-Cz2 horizon. The subround grains in all horizons abound with quartz carrying adhering particles, as shown in Fig. 7A, supporting with near duplicate imagery and EDS analysis, what was reported earlier by Mahaney (2015). In other cases, salt encrustations, adhering particles and microbes, as identified here, are similar to what was previously identified by Mahaney et al. (2001). The chemistry for the grain shown in Fig. 9B includes a quartz signature with minor Mg, Cl, K, S, and Fe but no carbon. Previously, Mahaney (2015, Fig. 8) reported subround grains dominating through the Ant-831 section, some with bulbous edges representative of aeolian transport (see Mahaney, 2002, for examples from other environments). Many grains in the Cz2 horizon carry striae on bulbous quartz suggesting that aeolian rounding preceded glaciation, with Mg–Ca sulphates covering striae further suggesting environmental transference: bedrock release → aeolian → glaciation → onset of dry climate.

4.5. Pebble pavement

Clast colors on pebbles within the Ant-831 pavement indicating salt encrustation are often mixed with dust of mica-illitic minerals, identified by XRD. Occasionally, salt encrustations are seen to carry silts close to clay dimensions, a mix of silicates, nitratine and gypsum as previously reported by (Mahaney and Schwartz, 2016) and reaffirmed here. Overturned pebbles often lose their salt encrustations but clasts with thick Na-encrusted surfaces often retain up to ~3 mm thickness and higher. The presence of thick Na-encrustations, along with thinner rims of salt on a clast, pale in color against the reddish-brown 5YR and 2.5YR hues of the remaining clast bulk-body. As shown in Fig. 3A–D, angular uncut clasts coated with variations of Si–Fe–Mn–Na minerals, provide an example of what samples look like after collection in the field. As colors darken, such coatings may contain fossil or extant microbes as suggested from other research into biotic elements in Antarctic paleosols (Mahaney et al., 2001; Hart et al., 2011). These salt-rich encrustations favor microbe growth by maintaining liquid water to well below freezing temperatures. Clast rind thickness in the Ant-831 pavement ranges from ~3 to ~15 mm; hence even the thinnest rinds and sand clasts occupy molecular space with a minimum 4×10^6 nm which is sufficient to house countless bacterial and fungal colonies. For microbe examples see Hart et al. (2011) and Mahaney et al. (2001); for clast example see Fig. 3 and similar imagery from the Mars Opportunity Rover (Mahaney et al., 2012).

Spatial separation of cold-humid from cold-dry climate may be seen at the Na-crust/weathered rock contact, although with thickening salt encrustation, movement of snowmelt into the weathering rind must slow down or stop. Thus, the early stage of rock weathering during the early Miocene probably continued uninterrupted for nearly the first half of the weathering period from ~30 Ma to ~15 Ma, slowing or ceasing after the MMCO (here the age control is middle Miocene). Following this line of reconstruction the salt-encrusted rind probably represents the most recent addition to the full rock weathering rind. With clast positions within the pavement and juxtaposition to the upper paleosol beneath, it is possible the bulk of available snowmelt was probably contained within these two mass areas.

The pebble pavement previously described by Mahaney et al. (2001) and Mahaney and Schwartz (2016) is important as an integral part of the sections at Aztec and New Mountain (Fig. 2B). Within these stratigraphic sections, the paleosol body yields important physical, mineral, and chemical data that assist in paleoenvironmental reconstruction, but on the physical side the pebble pavement provides even a higher level of information. For example, color changes down-profile within the paleosol body or bodies, as observed in the field are only gradual, one horizon to another, that is, with a uniform hue and only slight changes

down-section where values and chroma show only minor variation becoming lighter—higher value, lower chroma—down section away from the higher oxidation potential near the profile surface. As pointed out previously (Mahaney and Schwartz, 2016), nowhere is this more evident than previously reported color trends between the paleosol sections at Aztec and the New Mountain embayments (sites Ant-827, 828 and 829 in Mahaney et al., 2001) and the Alpine moraine high above the New Mountain embayment (site Ant-831). Clast colors within the pebble pavement in the younger group of sites at Aztec and the New Mountain embayment are within the 10YR 4/5 to 7.5YR 4/5 range, offset by the 5YR and 2.5YR stronger colors found on clasts within the older Alpine pebble pavement. While there are variations within each pebble group and variations within lithologies in each group, the dolerite carrying stronger hues in most cases, color is one of the most important physical parameters to be measured in the field. Clearly color is one of the most important parameters used to define variations between salt encrustations (high value, low chroma) and oxide-hydroxide active zones (lower value, lower chroma), and, in this instance, the latter colors suggest that the Alpine moraines are in a much older age-set than the Aztec and New Mountain embayment sections.

4.6. Source rock and glacigenic origin

Microtexture analysis of the sand fraction was carried out by SEM/EDS to determine relation to source rock and glacigenic origin. With respect to lithology, the Ant-831-Cox horizon composition carries a combination of quartz and feldspar minerals and dolerite rock fragments similar to other profiles (827–829) at Aztec and New Mountain, with approximately 60% quartz/feldspar and 40% dolerite. In the Ant-831 paleosol, horizons Cz1–5 yield almost the reverse percentages, with dolerite reduced to ~15–20% and quartz-feldspar greatly increased. Light microscope and SEM counts of about 300 grains per sample of fine and very fine sand support the reduction in dolerite below the Cox/Cz1 contact down-profile, so that the quartz/feldspar content in the 831-Cz1–5 horizons dilutes the total Fe concentration by a factor of approximately 3. Similarly, grain microtextures on section Ant-831 grains highlight a significant degree of grain rounding that contrasts greatly with grains imaged from the 827–829 sections where subround to round counts range from 40 to 60%. In the 831 profile about 75% of all grains imaged are classed as subround to round to a significant degree (Fig. 7A). However given proximity to outcrops of the Beacon Supergroup these figures should not be used to support warm based glaciation at Ant-831.

As reported by Mahaney (2015), representative quartz and orthoclase grains within the Cz stack of horizons are classed as subround, with quartz grains in the Cz2 horizon significantly covered with adhering silt particles and salts, the latter principally gypsum in composition. Detailed investigation of grains reveals copious V-shaped percussion cracks, nearly all heavily encrusted with salts, with the percussion fractures typically a common indicator of fluvial transport (Mahaney 2002; Mahaney et al., 2010; Costa et al., 2012). Moreover, these grains also carry a range of glacial-crushing microtextures, which include conchoidal and subparallel microfractures, deeper striations, many with variable depths partially covered with salts and Fe coatings. In some cases, multiple-cycle specimens carry a rock release to preweathered surface contrasted with fresher faces, the latter indicative of a complex history-release → first-order weathering → transport → overprinted weathering history. These grain coatings may also yield variable Si:Al ratios suggestive of 1:1 and 2:1 clays as well as thin Si, Al, and Fe coatings with variable but low C, the latter element likely related to secondary carbonate precipitation.

4.7. Rinds description and XRF chemical mapping

Examples of Fe- and Na-encrusted rinds are shown in Fig. 3A–D. The two Fe-encrusted rinds (Fig. 3A and B) are typical of clasts with Fe-

weathered rims composed of secondary oxides with only minimal Na-salts in places. Because the salt encrustation is variable on the clast surface it is impossible to tell just what the x-y clast attitude dimensions have been over time but the weathered surface is near continuous over both samples, so it is possible the clasts may have changed positions within the pavement. While we do not know the density of both specimens, it is possible the clast angle observed is case hardened, thus capping rind development (Dorn et al., 2017). The other two examples (Fig. 3C and D) are more typical of rinds in the pavement, both with salt cap encrustations overlying the remainder of rind development into the clastic core rock. The sample (Fig. 3C) shows thin stratification in the sandstone with a relatively clean salt-encrusted mass capping the clast. The example in Fig. 3D differs with a thicker salt encrustation with intermixed rind detritus sourced from physical and/or chemical weathering of nearby clasts or from airfall influx, source unknown.

The annotated rind in Fig. 4 shows the rind and core marked areas in the clast and gives a representative view into the sandstone showing a mix of subround to subangular grains, all of medium to very coarse grade size (250–2000 μm), and with a few approaching round status. The image depicts minor stratification near the clast top but otherwise grains are separated by rather wide matrices mostly filled with mica and illite materials. The rind edge may be case-hardened and this may explain the segregated salt distribution through the outer rind mass.

Using Micro X-ray fluorescence EDAX spectrometry, the chemical maps (Fig. 4B) provide the distribution of Si with Al–Fe–S taking up the matrix areas, which matches the generic composition of the Beacon sandstone. On these chemical maps Si is the dominant element and corresponds to quartz grains while the matrix is dominated by high content of Al and Fe corresponding to the clay phases. Sulphur, limited to the right margin (Fig. 4B) with other undefined salts, may be sourced by weathering of gypsum or from volcanic emissions.

4.8. XRD analyses

The bulk (Fig. 5A) and clay (Fig. 5B) rind fractions were characterized in order to determine the mineralogical phases and their relation to weathering in the paleosol. The bulk fraction shows that the sample is dominated by quartz (82.4%) embedded within a matrix composed with the association of chlorite (3%), interstratified chlorite/illite (10.4%) and iron oxides (3.6%). The iron oxides correspond to hematite (1%) and goethite (2%) and small amount of magnetite (0.6%). The hematite and goethite bulk concentrations within the rind more than double that of the paleosol horizons as shown in Table 1, which may indicate that water retention in the pebble pavement is higher than originally thought. The XRD diffractograms of the clay fraction show that the major clay phases correspond to chlorite/illite interstratified and illite.

4.9. SEM/EDS

The SEM analyses of the pavement in Ant-831 (Fig. 6) show that the sample corresponds to round/subround grains of quartz embedded with a matrix. The quartz grains develop irregular shapes related to weathering processes (Fig. 6B and C) producing the interlocking structure between some quartz crystals (Fig. 6D). The weathering is also observed in the matrix where the chlorite and illite were replaced by illite/chlorite interstratified and by the development of Fe-oxide/hydroxide corresponding to hematite and goethite located at the quartz boundary (Fig. 6D).

SEM and EDS analyses of grains recovered from the Ant-831 paleosol, particularly the Cz2 horizon, reveal paleoecologic and paleoclimatic evidence of former glaciation followed by tundra-like conditions that existed at some point during paleosol morphogenesis. The bulk of the sediment recovered and analyzed from the paleosol varied from dolerite heavy grains in the surface Cox horizon, reverting to quartz-feldspathic lithologies at depth produced a wealth of round to subangular grains in both categories, as for example, the image and chemistry in Fig. 7A–B.

The image shows craters of variable dimension in a coarse sand surface about ~700 μm diameter, near parabolic striae infilled with adhering particles, and scattered v-shaped percussion cracks that suggest a mixed transport by ice and water, the median subround state common amongst the grains analyzed. The chemistry shows the grain is quartz, with minor orthoclase indicated from adhering particles along with a thin Fe coating. The sample was examined under low pressure; hence the absence of carbon.

Aside from the copious fossil Coleoptera recovered from the Cz2 horizon (Mahaney, 2015), the fossil plant remains of preserved grass-sedge and other unspecified and unclassified vascular plant remains are nearly as common as recovered mineral grains. The image and chemistry in Fig. 8A–B shows intertwined root particles of fine silt size diameter with adhering particles that appear feldspathic given the abundant K with lesser Si:Al (=2:1). Abundant Cl and K suggest the fossil plant is rich in sylvite and perhaps in secondary Si coating. The C registered is real since the sample was analyzed without coating. Additional examples of plant occupants of a former tundra paleoenvironment come from Fig. 9A–B and 10A-B. In Fig. 9A, a pithy-woody fossil with heavy incorporated gypsum, minor orthoclase particles and trace of Fe coating are particularly numerous in the Cz2 horizon, the gypsum a common dry climate product. The image in Fig. 10A presents a common occurrence of inter-bound rootlets encased in mineral matter, presumably Ca-plagioclase and/or minor orthoclase and gypsum with Fe coatings. Examples of intertwined rootlets are commonly found with fossil Coleoptera (Mahaney, 2015).

4.10. Paleoecology

Of all evidence for an ameliorative climate in the MMCO or before, the imagery and chemistry in Figs. 8A–B, 9A-B and 10A-B place the paleoecological evidence in support of a tundra environment. Fig. 8A shows 15 μm wide double rootlets, possibly of a vascular plant with small carbon remaining, and as indicated by EDS, the sample carries sylvite salts with adhering particles of K-spar. Fossil wood from the Cz2 horizon differs from Fig. 8A (EDS Fig. 8B), showing gypsum as the major salt with accessory K-spar and Fe, most likely Fe^{+3} coating. The absence of C suggests all carbon was lost to the carbon cycle at some point in the fossilization process. Fig. 10A depicts a rootlet mat of material, part organic with encrusted inorganic material, the small carbon imprint suggesting again some loss with weathering. The presence of low Fe and stronger Na–Ca salts indicate that most salt concentration probably occurred after the MMCO. Because EDS analysis highlights minor concentrations of Al, Mg, Na, K, Cl, and Fe indicating that salts are present, such may be responsible for maintaining water in liquid form allowing Fe^{+3} to form on occasion and microbes to proliferate. As pointed out above, because pyrophosphate Al (Al_p) is considered a proxy for organic carbon (Parfitt and Childs, 1988; Mahaney et al., 2014), this test correlating Al_p with organic carbon (Table 1) shows that even minor concentrations of Al_p throughout the Ant-831 section do not always correlate with measurement of organic carbon (i.e. the Cz2 and Cz4 horizons); thus, it may not always provide a reliable proxy for organically-complexed compounds.

4.11. Weathering and paleoclimate histories

Assuming that weathering began at some point after emplacment of the moraine and its clast-heavy surface that became the pebble pavement following a winnowing of fine-grain sediment and onset of physical and chemical weathering, horizon ordering top to bottom in the paleosol, suggests the Cox/Cz1 horizons were the weathering starting point in paleosol morphogenesis. The occurrence of fossil Coleoptera and plant/root material, all intertwined with clay, Fe, and evaporite minerals suggests the Cz2 horizon developed later, perhaps with the advent of the cold-humid climate of the early Miocene becoming somewhat warmer and possibly with more moisture favoring the development of a tundra environment, perhaps with dimensions similar to what exists now along the Antarctic coast. Further deepening and development of the Ant-831 paleosol to include the Cz3 and Cz4 horizons, presumably over the 15 Myr time from the MMCO to the present, incorporates the final, full stage of weathering from its inception at the late Oligocene/early Miocene transition. This includes the reconstruction of the slow trend of cold-humid to cold-dry climate that produced the Ant-831 pedostratigraphic complex, in microcosm, similar to the inferred macrocosm of cool humid to cold-dry Noachian-Amazonian transfer of paleoclimate on Mars (Mahaney et al., 2012).

The abrupt climatic cooling and onset of cold-dry climate in the Antarctic Dry Valleys, estimated at 14 Ma by Lewis et al. (2008), mark the disappearance of tundra vegetation including fossilized plants and insects. Compared with a survey of sediment recovered from sites in the New Mountain embayment, dated to ~15 Ma, that did not produce any fossilized biotic material may indicate that the 14 Ma age is somewhat younger than the cold-dry lockdown of the Inland Ice Sheet as estimated here. However, it does support the occurrence of earlier fossilized remains discovered in Alpine-age sediment at higher elevations on the flanks of New Mountain when a tundra environment existed.

5. Conclusions

Looking into a ~30 Myr window incorporated into thin lamina of clasts may not have the precision of ice and marine core analyses, but nevertheless, both paleosols in glacial drift, and/or clasts in pebble pavements yield considerable data, not only on weathering processes, but also on the transition from cold-humid to cold-dry Antarctic paleoclimates. The sandstone clast analyzed here is probably from the Hatherton member of the Beacon Supergroup, scoured and transported to site by the one of the earliest glaciers to occupy the high areas in the Transantarctic Mountains (Aztec Mountain and New Mountain areas), offering up the opportunity to analyze the inner sandstone with individual sand clasts visible as to roundness, lack of sorting and stratification but with the sum total of coatings and their chemical compositions. The inverted salt to oxihydrite-rich weathering zones in the pebble clast, to adjoined paleosol with its oxihydrite-rich surface horizon trending to salt-rich horizon at depth, supports not only what has been shown by laboratory experimentation to be salt ionic transference but also that salt accumulations became more prominent with the change in climate from cold-humid to cold-dry, all presumably occurring at the 15 Ma-MMCO or at some other point in the middle Miocene, i.e. 14 Ma (Lewis et al., 2008). It is also possible, given late Miocene ages of the cold-dry ice lockdown, recently advanced by Dickenson et al. (2012), that the early Alpine glaciation lasted longer than many workers believe.

Looking deeper into this ~30 Myr window, it is apparent that weathered clast rinds offer a complimentary paleoenvironmental record compared to paleosols, and also that rinds are favored to some degree since they cannot respond to profile transport forces such as exist in finer-grained substrates. In polar environments, especially extremely cold environments, clasts in pebble pavements tend to maintain their x-y coordinates as indicated by the orientation of salt crusts to weathered clast bodies, top to bottom. The collection of clasts that form the pavement in most moraines probably represent clast-heavy basal ice that, once emplaced, is probably winnowed of fines following withdrawal of ice. Thus, the pavement settles into the finer-grained substrate, the entire paleosol mass, bolstered by the presence of dry frozen conditions, tends to maintain partly convoluted horizon boundaries, as in many Gelisols. Thus, while some polar soils contain enough fine-grained material, especially expandable clay minerals, to produce parabolic horizon boundaries, others with coarser-grained textures including boulders and cobbles, such as the pedon described here, tend to form profiles that grow downward with horizon boundaries oriented around large clasts.

Assessment of the advanced age for the Ant-831 section, in comparison with sites Ant-828 and Ant-829 in the lower New Mountain

embayment, rests partly upon the weathered sediment/clast rind colors that are supported by more robust chemical Fe extractions, SEM imagery, EDS and XRF analyses. More to the point, the presence of cold warm fossilized tundra vegetation and insect remains not found in other sites at New Mountain and Aztec Mountain (despite a thorough search of recovered samples) support an older Alpine age.

Declaration of competing interest

The authors declare that they have no known competing financial interests or personal relationships that could have appeared to influence the work reported in this paper.

Acknowledgements

References

Anderson, J.B., Warny, S., Askin, R.A., Wellner, J.S., Bohaty, S.M., Kirshner, A.E., Livsey, D.N., Simms, A.R., Smith, T.R., Ehrmann, W., Lawyer, L.A., Barbeau, D., Wise, S.W., Kulhenek, D.K., Weaver, F.M., Majewski, W., 2011. Progressive Cenozoic cooling and the demise of Antarctica's last refugium. PNAS, early edition 1–5.

Armstrong, R.L., 1978. K–Ar dating: late Cenozoic McMurdo volcanics and Dry Valley glacial history. N. Z. J. Geol. Geophys. 21, 685–698.

Barrett, P.J., 1981. History of the Ross Sea region during the deposition of the Beacon Supergroup 400 - 180 million years ago. J. Roy. Soc. N. Z. 11, 447–458.

Birkeland, P.W., 1974. Use of relative age dating methods in a stratigraphic study of rock glacier deposits, Mt. Sopris, Colorado. Arct. Alp. Res. 5 (4), 401–416.

Birkeland, P.W., 1999. Soils and Geomorphology. Oxford University Press, Oxford, U.K., p. 430

Bo, S., Siegert, M.J., Mudd, S.M., Sugden, D., Fujita, S., Xiang, C., Xueyuan, T., Yuansheng, L., 2009. The Gamburtsev mountains and the origin and early evolution of the Antarctic Ice Sheet. Nature 459. https://doi.org/10.1038/nature08024.

Bockheim, J.G., 2007. Soil processes and development rates in the quartermain mountains, upper Taylor Glacier region, Antarctica. Geogr. Ann. 89, 153–165.

Bockheim, J.G., 2013. Paleosols in the transantarctic mountains: indicators of environmental change. Solid Earth Discussions 5, 1007–1029.

Bradshaw, M., 2013. The Taylor group (Beacon Supergroup), the Devonian sediments of Antarctica. J. Geol. Soc. https://doi.org/10.1144/SP381.23.

Campbell, I.B., Claridge, G.G.C., 1987. Antarctica: Soils, Weathering Processes and Environment. Elsevier, Amsterdam., p. 368

Claridge, G.G.C., 1977. The salts in Antarctic soils, their distribution and relationship to soil processes. Soil Sci. 123, 377–384.

Claridge, G.G.C., Campbell, I.B., 1968. Origin of nitrate deposits. Nature 217, 428–430.

Costa, P.J.M., Andrade, C., Dawson, A.G., Mahaney, W.C., Freitas, M.C., Paris, R., Taborda, R., 2012. Microtextural characteristics of quartz grains transported and deposited by tsunamis and storms. Sediment. Geol. 275–276, 55–69.

Cuffey, K.M., Conway, H., Gades, A.M., Hallet, B., Lorrain, R., Severinghaus, J.P., Steig, E.J., Vaughn, B., White, J.W.C., 2000. Entrainment at cold glacier beds. Geology 28 (4), 351–354.

Dickenson, W., Schiller, M., Ditchburn, R., Graham, I., Zondervan, A., 2012. Meteoric Be-10 from Sirius group guggests high elevation McMurdo dry valleys permanently frozen since 6 Ma. Earth Planet Sci. Lett. 355–356, 13–19.

Denton, G.H., Anderson, R.F., Toggweiler, J.R., Edwards, R.L., Schaefer, J.M., Putnam, A.E., 2010. The last glacial termination. Science 328 (5986), 1652–1656.

Dorn, R.I., Mahaney, W., Krinsley, D.H., 2017. Case hardening: turning weathering rinds into protective shells. Elements 13, 165–169.

Eglinton, T.I., 2012. A rusty carbon sink. Nature 483, 165–166.

Ferrar, H.T., 1907. Report on the field geology of the region explored during the *Discovery* Antarctic Expedition 1901-1904. Nat Antarct. Exped. 1901-1904. Nat. History 1, 1–100.

Graham, I.J., Ditchburn, R.G., Claridge, G.G.C., Sheppard, D.S., Whitehead, N.E., Xondervan, A., Sheppard, D.S., 2002. Dating Antarctic soils using atmosphere-derived [10]Be and nitrate. In: Gamble, J.A., Skinner, D.N.B., Henry, S. (Eds.), Antarctica at the Close of a Millennium: Proc. 8th Int. Symposium on Antarctic Earth Sciences, pp. 429–436.

Guglielmin, M., Cannone, N., Strini, A., Lewkowicz, A.G., 2005. Biotic and abiotic processes on granite weathering landforms in a cryotic environment, Northern Victoria Land, Antarctica. Permafr. Periglac. Process. 16 (1), 69–85.

Hancock, R.G.V., 1984. On the source of clay used for Cologne Roman pottery. Archaeometry 26, 210–217.

Harrison, T.P., Hancock, R.G.V., 2005. Geochemical analysis and sociocultural complexity: a case study from early Iron Age Megiddo (Israel). Archaeometry 47, 705–722.

Hart, K.M., Szpak, M.T., Mahaney, W.C., Frazer, A.R., Jordan, S.F., Dohm, J.M., Allen, C.R., Kelleher, B.P., 2011. Bacterial enrichment study and overview of the extractable lipids from Antarctic paleosols, Dry Valleys, Antarctica. Astrobiology 11, 303–321.

Hodgson, J.M., 1976. Soil Survey Field Handbook. Soil Survey Tech. Monograph No. 5. Rothamsted Experimental Station, Harpenden, Herts, UK, p. 99.

Lewis, A.R., Marchant, D.R., Ashworth, A.C., Hemming, S.R., Machlus, M.I., 2007. Major middle Miocene global climate change: evidence from East Antarctica and transantarctic mountains. Geol. Soc. Am. Bull. 119, 1449–1461.

Lewis, A.R., Marchant, D.R., Ashworth, A.C., Hedena, L., Hemming, S.R., Johnson, J.V., Leng, M.J., Machlus, M.L., Newton, A.E., Raine, J.I., Willenbring, J.K., Williams, M., Wolfe, A.P., 2008. Mid-Miocene cooling and the extinction of tundra in continental Antarctica. Proc. Natl., Academy of Sciences 105 (31). https://doi.org/10.1073/pnas.0802501.105.

Link, A.G., 1966. The textural classification of sediments. Sedimentology 7 (3), 249–254.

Lutwick, L.E., Dormaar, J.F., 1973. Fe status of Brunisolic and related soil profiles. Can. J. Soil Sci. 53, 85–97.

Mahaney, W.C., 1978. Late quaternary stratigraphy and soils in the wind river mountains, western Wyoming. In: Mahaney, W.C. (Ed.), Quaternary Soils. Norwich, Geoabstracts, pp. 223–264.

Mahaney, W.C., 1990. Ice on the Equator. Wm Caxton, Ellison Bay, Wi, p. 386.

Mahaney, W.C., 2002. Atlas of Sand Grain Surface Textures and Applications. Oxford University Press, Oxford, UK, p. 237.

Mahaney, W.C., 2015. Pedological iron/Al extracts, clast analysis and Coleoptera from Antarctic paleosol 831: evidence of a middle Miocene or earlier climatic Optimum. J. Geol. 123, 113–132.

Mahaney, W.C., 2019. Paleoenvironmental archives in rock rinds and sand/silt coatings. J. Geol. 127, 411–436.

Mahaney, W.C., Keiser, L., 2013. Weathering rinds-unlikely host clasts for an impact-induced event. Geomorphology 184, 74–83.

Mahaney, W.C., Schwartz, S., 2016. Paleoclimate of Antarctica reconstructed from clast weathering rind analysis. Palaeogeogr. Palaeoclimatol. Palaeoecol. 446, 205–212.

Mahaney, W.C., Dohm, J.M., Baker, V.R., Newsom, H.E., Malloch, D., Hancock, R.G.V., Campbell, I., Sheppard, D., Milner, M.W., 2001. Morphogenesis of Antarctic paleosols: martian analogue. Icarus 154, 113–130.

Mahaney, W.C., Dohm, J.M., Kapran, B., Hancock, R.G.V., Milner, M.W., 2009. Secondary Fe and Al in Antarctic paleosols: correlation to Mars with prospect for the presence of life. Icarus 203, 320–330.

Mahaney, W.C., Dohm, J.M., Fairien, A., 2012. Weathering rinds on clasts: examples from Earth and Mars as short and long term recorders of paleoenvironment. J. Planet. Space Sci. 73, 243–253.

Mahaney, W.C., Krinsley, D., Kalm, V., 2010. Evidence for a cosmogenic origin of fired glaciofluvial beds in the northwestern Andes: correlation with experimentally heated quartz and feldspar. Sediment. Geol. 23, 31–40.

Mahaney, W.C., Keiser, L., Krinsley, D.H., Pentlavalli, P., Allen, C.C.R., Somelar, P., Schwartz, S., Dohm, J.M., Dirszowsky, R., West, A., Julig, P., Costa, P., 2013. Weathering rinds as mirror images of palaeosols: examples from the Western Alps with correlation to Antarctica and Mars. J. Geol. Soc. 170, 833–847.

Mahaney, W.C., Krinsley, D.H., Razink, J., Fischer, R., Langworthy, K., 2016. Clast rind analysis using multi-high resolution instrumentation. Scanning 9, 1–11.

Mahaney, W.C., Krinsley, D.H., Milner, M.W., Fischer, R.F., Langworthy, K., 2018. Did the black mat impact/Airburst reach the Antarctic: evidence from new mountain near the Taylor Glacier in the Dry Valley mountains. J. Geol. 126 (3), 285–305.

Mahaney, W.C., Schwartz, S., Hart, K., Dohm, J., Allen, C.C.R., 2014. Mineralogy, chemistry and biological contingents of a Early-Middle Miocene Antarctic paleosol and its relevance as a Martian analogue. J. Planet. Space Sci. 104, 253–269.

Marchant, D.R., Denton, G.H., Sugden, D.E., Swisher III, C.C., 1993. Miocene glacial st rati- graphy and landscape evolution of the western Asgard Range, Antarctica. Geografisker Annaler 75A, 303–330.

Mehra, O.P., Jackson, M.L., 1960. Iron oxide removal from soils and clays by a dithionite-citrate system buffered with sodium bicarbonate. In: National Conference on Clays and Clay Minerals, 1958. Pergamon, London, pp. 317–327.

Millar, C.E., Turk, L.M., Foth, H.D., 1966. Fundamentals of Soil Science, fourth ed. Wiley, N.Y., p. 491

National Soil Survey Center (NSSC), 1995. Soil Survey Laboratory Information Manual. Soil Survey Investigations Report No. 45, p. 305 version 1.00, U.S.D.A.

Nelson, R.L., 1954. Glacial geology of the frying Pan river drainage, Colorado. J. Geol. 62, 325–343.

Owen, L.A., Thackray, G., Anderson, R.S., Briner, J., Kaufman, D., Roe, G., Pfeffer, W., Yi, C.L., 2009. Integrated research on mountain glaciers: current status, priorities and future prospects. Geomorphology 103, 158–171.

Oyama, M., Takehara, H., 1970. Standard Soil Color Charts. Japan Research Council for Agriculture, Forestry and Fisheries, Tokyo.

Parfitt, R.L., Childs, C.W., 1988. Estimation of forms of Fe and Al: a review and analysis of contrasting soils by dissolution and Moessbauer methods. Aust. J. Soil Res. 26, 121–144.

Passchier, S., 2004. Variability in geochemical provenance and weathering history of Sirius Group strata, Transantarctic Mountains: implications for Antarctic glacial history. J. Sediment. Res. 74, 607–619.

Passchier, S., 2011. Climate change: ancient Antarctic fjords. Nature 474, 46–47.

Seybold, C.A., Harms, D.S., Balks, M., Aislabie, J., Paetzold, R.F., Kimble, J., Sletten, R., 2009. Soil climate monitoring project in the Ross Island region of Antarctica. Soil Horiz. 50, 52–57.

Sharp, R.P., 1969. Semiquantitative differentiation of glacial moraines near Convict lake, Sierra Nevada, Calif. J. Geol. 77, 68–91.

Shaw, S.E., 1962. Petrography of Beacon sandstone samples from Beacon height west, upper Taylor Glacier, Antarctica. N. Z. J. Geol. Geophys. 5, 733–739.

Soil Survey Staff, 1999. Soil Taxonomy. USDA, Agric. Handbook No. 436. Gov't Printing Office, Washington).

Stewart, Duncan, 1934. Petrography of the Beacon sandstone of South Victoria Land. Am. Mineral. 19, 351–359.

Ugolini, F.C., Anderson, D.M., 1973. Ionic migration and weathering in frozen Antarctic soils. Soil Sci. 115, 461–470.

Warny, S., Askin, R.A., Hannah, M.J., Mohr, B.A.R., Raine, J.I., Harwood, D.M., Florindo, F., the SMS Science Team, 2009. Palynomorphs from a sediment core reveal a sudden remarkably warm Antarctic during the Middle Miocene. Geology 10, 955–958.

Wilson, A.T., 1973. The great antiquity of some Antarctic landforms. Evidence for an Eocene temperate glaciation in the McMurdo region. In: van Zinderen Bakker, E.M. (Ed.), Palaeoecology of Africa. Balkema, Capetown, pp. 23–35.

Wunderling, N., Willeit, M., Donges, J.F., Winkelmann, R., 2020. Global warming due to loss of large ice masses and Arctic summer sea ice. Nat. Commun. 11, 5177.

Wynn-Williams, D.D., Edwards, H.G.M., 2000. Proximal analysis of regolith habitats and protective biomolecules in site by Raman Spectroscopy: overview of terrestrial Antarctic habitats and Mars analogy. Icarus 144 (2), 486–503.